American Journal of Electrical and Computer Engineering
2020; 4(2): 35-48
http://www.sciencepublishinggroup.com/j/ajece
doi: 10.11648/j.ajece.20200402.12
ISSN: 2640-0480 (Print); ISSN: 2640-0502 (Online)

Voltage-Frequency Control (v-f) of Islanded Microgrid Based on Battery and MPPT Control

Masoud Dashtdar, Majid Dashtdar

Electrical Engineering Department, Bushehr Branch, Islamic Azad University, Bushehr, Iran

Email address:
dashtdar.masoud@gmail.com (Masoud D.), dashtdar.m@gmail.com (Majid D.)

To cite this article:
Masoud Dashtdar, Majid Dashtdar. Voltage-Frequency Control (v-f) of Islanded Microgrid Based on Battery and MPPT Control. *American Journal of Electrical and Computer Engineering.* Vol. 4, No. 2, 2020, pp. 35-48. doi: 10.11648/j.ajece.20200402.12

Received: April 12, 2020; **Accepted**: April 24, 2020; **Published**: August 25, 2020

Abstract: With the development and increasing influence of the use of distributed generation resources, distribution networks have changed from passive networks to active networks. In these new networks, operation on an island will increase both the reliability of the network in the competitive market and the maximum utilization of distributed generation resources. But despite the various benefits, Microgrids with distributed generation resources also have disadvantages. One of the disadvantages is the increasing complexity of control systems, protection systems and operating systems of the global distribution network. In recent research, various methods have been proposed for controlling the Microgrids, especially voltage and frequency control. This paper presents a method for controlling a photovoltaic (PV) system with maximum power point tracking (MPPT) controller and battery storage to provide voltage-frequency (v-f) support in an islanded microgrid. It introduces a new algorithm for MPPT control that offers control strategies, effective coordinated between v-f control in inverter, MPPT control, and battery storage control. Finally, the proposed scheme is implemented on the IEEE 13-bus distribution feeder in islanded mode using MATLAB software, the results of which clearly demonstrate the efficiency of the control methods.

Keywords: Distributed Energy Sources (DER), Distributed Generation (DG), Maximum Power Point Tracking (MPPT), Voltage-Frequency Control (v-f), Photovoltaic System (PV)

1. Introduction

With the increasing use of electricity worldwide, the electricity industry has faced issues such as the high cost of building new power plants and the development of transmission, distribution networks, environmental concerns, and climate change. In order to overcome these problems, increase customer service reliability and reduce congestion and loss in transmission and distribution lines, distributed and renewable energy sources are new and viable options introduced over the last two decades [1]; Renewable energy has led to their planning for greater use in the electricity industry and the increasing expansion of Microgrids in most countries worldwide [2]. Microgrids are small power networks made up of several renewable energy sources and local loads. Microgrids are normally connected to one of the distribution network buses, but in an emergency, if large disturbances occur, they are disconnected from the power network and feed some loads (critical loads). In this regard, the use of solar energy is of great importance, and PV systems have been widely used as a source of distributed generation in Microgrids [1].

Microgrids include distributed generation units, energy storage systems and electrical loads, operated as a standalone, controllable system capable of providing power and heat to local customers [2]. The Point of Common Coupling (PCC) is connected to the mains voltage through a power breaker circuit. In islanded mode, the Microgrid must be capable of controlling voltage and frequency independently of the grid and thus operate as a P-V (power-voltage) bus.

Similar to the traditional frequency control method in the synchronous generator [3], the Microgrid voltage and frequency control can also be performed using drop control methods [4-8]. The present study provides a faster response for voltage and frequency control than the secondary control discussed in [8]. A comparison between inverter control and synchronous generator control in an islanded microgrid is presented in detail [9]. Operating and controlling the inverter

connected to the distribution of renewable energy sources such as a PV system in a Microgrid is particularly challenging to maintain within acceptable voltage-frequency range. The voltage control method based on classical drop control for voltage drop has been studied [10].

In the field of voltage-frequency control using a PV system with MPPT control and battery storage in Microgrid, there is a lack of research. Frequency control using a PV system is studied in a Microgrid, although voltage control is not the purpose of the paper and does not include an energy storage system [11].

In summary, previous research has not performed well in view of the involvement of energy storage devices in the field of voltage control coupled with frequency tuning or the consideration of control modes in different scenarios. In the present study, taking into account these shortcomings as well as eliminating the calculation of the transition between the reference frame abc to dq0 and unlike, it attempts to provide better results than in the past.

The Continue of this paper is organized as described in Section 2, Solar Array Analytical Modeling, PV system configuration and battery modeling, outlines the relevant control algorithms in Section 3, Section 4 contains the Microgrid description understudy. The results of the simulation will be followed by a final conclusion in Section 5.

2. Describe the System Under Study

In this section, the various components of the system under study will be described in detail.

2.1. Solar PV Modeling

The generally accepted model for solar cells is the single-diode model [12]. The present paper uses a single-diode model for a solar cell in the Kyocera KC200GT solar array shown in Figure 1. The V-I characteristic of a solar array is obtained from Equation (1) according to Figure 1:

$$I = I_{pv} - I_o\left[exp\left(\frac{V+R_sI}{V_{therm}\alpha}\right) - 1\right] - \frac{V+R_sI}{R_{sh}} \quad (1)$$

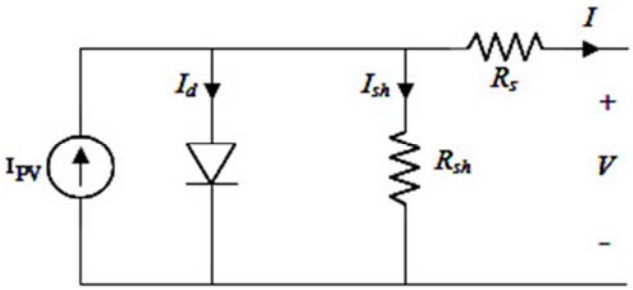

Figure 1. *Single-diode equivalent circuit of PV cell [12].*

Where I_{PV} and I_o are represented photon and diode saturation currents, respectively. V_{therm} is the thermal voltage of the array, R_S and R_{Sh} respectively of series and parallel resistors and α is the ideal coefficient which is usually chosen between 1 and 1.5 and is assumed to be 1 here. The characteristic V-I, KC200GT for different levels of radiation at 25°C cell temperature is shown in Figure 2. The consistency of the above graphs with the datasheet confirms the validity of the model used. The parameters of the solar panel are presented in Table 1.

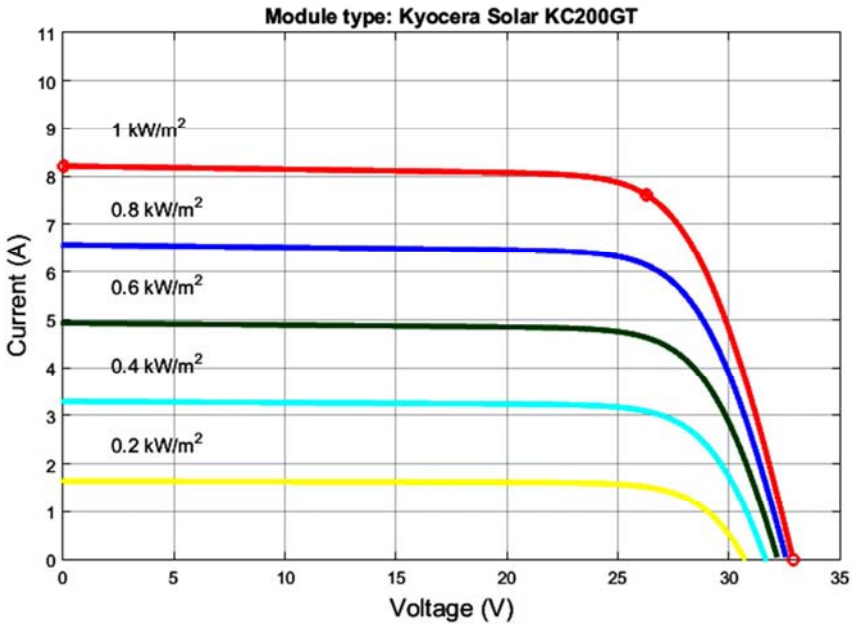

Figure 2. *I-V characteristic of the Kyocera KC200GT Panel derived from simulation for different levels of radiation.*

The PV panel understudy has 125 strands in 4 series. The maximum power point (MPP[2]) for a panel at a radiation level of 1000 W/ m^2 and at 25°C (STC[3]) is 200 W and therefore 100 kW for the total system. MPP will change with changes in radiation levels and cell temperature.

Table 1. *PV Panel Parameters in STC [15].*

Model	Kyocera KC200GT
P_{MPP}	200 W
V_{MPP}	26.30 V
I_{MPP}	7.61 A
V_{OC}	32.90 V
I_{SC}	8.21 A

2.2. PV System Configuration

As shown in Figure 3, the system has a two-level configuration that uses a DC-DC converter to control MPPT. There is also battery storage for emergencies and maintaining voltage and frequency of the grid or providing critical loads. The battery is connected to the PV in order to inject or absorb the active power through a DC-DC bidirectional converter. When the battery absorbs power, the converter operates in a reduced state and when injected into the grid, in an incremental state.

The PV system is connected to the network through the Lc inductance. This inductance eliminates the distortions of the PV output current. The connection point is called PCC and its voltage is $V_c(t)$. The rest of the system is a 13-bus IEEE distribution feeder, which is modeled as an impedance station equivalent to R+jwLs. The PV source is connected to the DC inverter through the C_{dc} capacitor. PV is the active power source and the capacitor is the reactive power source.

According to the instantaneous power definitions for a balanced three-phase system assuming no harmonics, if $V_t(t)$ and $V_C(t)$ respectively represent the PCC instantaneous voltage and the inverter output voltage, then the average active and reactive power of the PV system is P(t) and Q(t) will be calculated as follows [13]:

$$P(t) = \frac{2}{T}\int_{t-T/2}^{t} vt(\tau)ic(\tau)d\tau = \frac{Vt(t)Vc(t)}{\omega Lc} sin\alpha \qquad (2)$$

$$Q(t) = \frac{Vt(t)}{\omega Lc}(Vc(t)cos\alpha - Vt(t)) \qquad (3)$$

Where α is the angle of phase $V_C(t)$ relative to the voltage of PCC. If the angle α is small, P(t) and Q(t) in Equation (2) and Equation (3) can be estimated with the first component of the Taylor series and arrive at the following equations:

$$P(t) \approx \frac{Vt(t)Vc(t)}{\omega Lc}\alpha \qquad (4)$$

$$Q(t) = \frac{Vt(t)}{\omega Lc}(Vt(t) - Vc(t)) \qquad (5)$$

2.3. Battery Modeling

Due to the variable nature and the uncertainty in solar power generation as well as the extreme load fluctuations, full-cycle lead-acid batteries are used. Battery charging limitations are also provided for 20% discharge and 80% recharge. The accurate details of the battery model are given in [14], which is an analytical type with two equations for the discharge and charge states. In this model, to model open-circuit voltage, a term for voltage and resistance polarization is considered that makes it much more accurate.

The battery charge and discharge relationships are expressed in Equation (6) and Equation (7) respectively:

$$V_{batt} = Vo - R.i - K\frac{Q}{Q-it}(it + t^*) + Exp(t) \qquad (6)$$

$$V_{batt} = Vo - R.i - \left[K\frac{Q}{it-0.1Q}\right]i^* - \left[K\frac{Q}{Q-it}\right].it + Exp(t) \qquad (7)$$

Where, V_{batt}: Battery voltage, V_o: Battery constant voltage, K polarization constant (V/Ah) or polarization resistance (Ω), Q Battery capacity (Ah), it = ∫I dt Actual battery charge (Ah), A is exponential zone amplitude (V), B exponential zone time constant inversion (Ah^{-1}), R internal resistance (Ω), i battery current (A), and i* filtered Current (A).

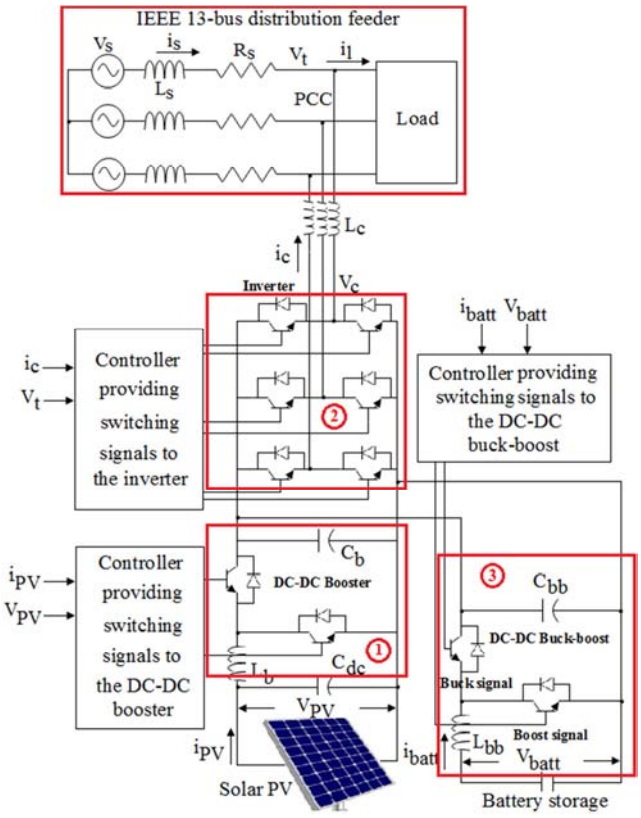

Figure 3. *Configuration of a PV system with MPPT and battery [15].*

In Equation (7), the first and second brackets represent the polarization resistance and the polarization voltage, respectively. The size of the battery is selected so as to be able to compensate for the failure of the PV system to produce under conditions very low or zero irradiation and provide maximum power point. In this, the MPP in the STC is 100 kW and therefore the battery should be able to provide this power for up to 1 hour.

Because the battery is intended for short-term applications such as frequency control or critical load emergency response, it provides one-hour support for any other generator to handle frequency control or balance the power in the Microgrid, which will be sufficient.

3. Expression of Control Methods

In this section, the control methods considered for the photovoltaic system will be investigated in the present study.

3.1. MPPT Control Algorithm

Given the high cost and low efficiency of the PV system, it is desirable that the solar array is always operated at a given radiation level and temperature and at the highest possible power. This control is known as the MPPT. Operating the PV system at the maximum power point (MPP) can be used when connecting to the network to support the network by providing clean energy and avoiding the installation of costly energy storage systems. As such, MPP-sized loads will be supplied by solar power and the remainder of the electrical loads by the power network. The P-V curves of the KC200GT solar panel for different radiation levels and variable temperatures are shown in Figures 4 and 5, respectively. Figures 6 and 7 also show the relationship between the solar panel's maximum power point (MPP) and the radiation level and cell temperature, respectively. It is clear that MPP with radiation levels, directly and inversely with temperature cells, and in both cases the relationship is linear. So it is logical to use a table with linear estimation to find non-existent data.

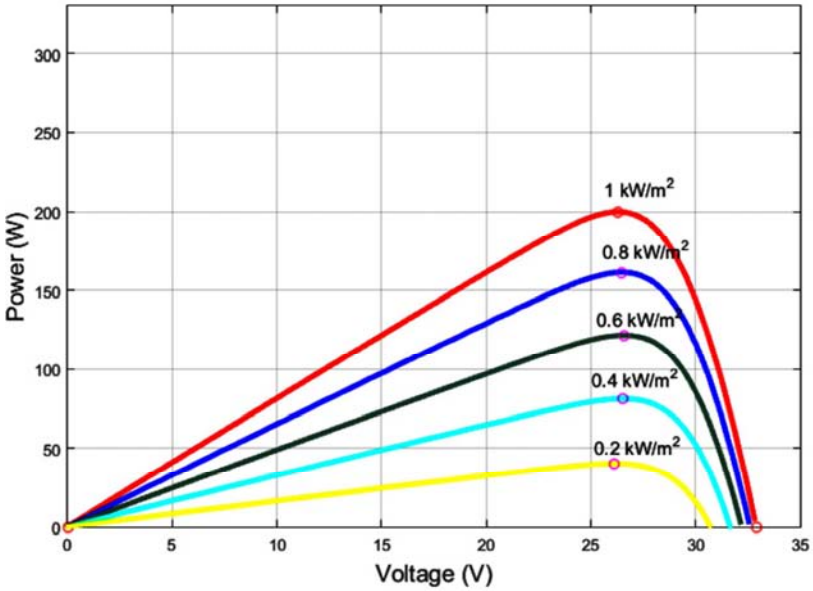

Figure 4. *PV curve of solar panel KC200GT due to radiation level change.*

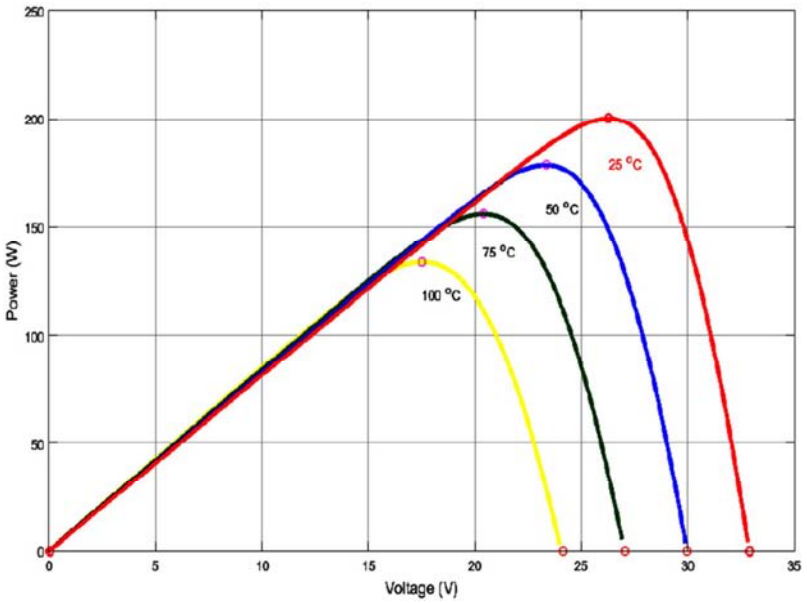

Figure 5. *PV curve of solar panel KC200GT due to cell temperature change.*

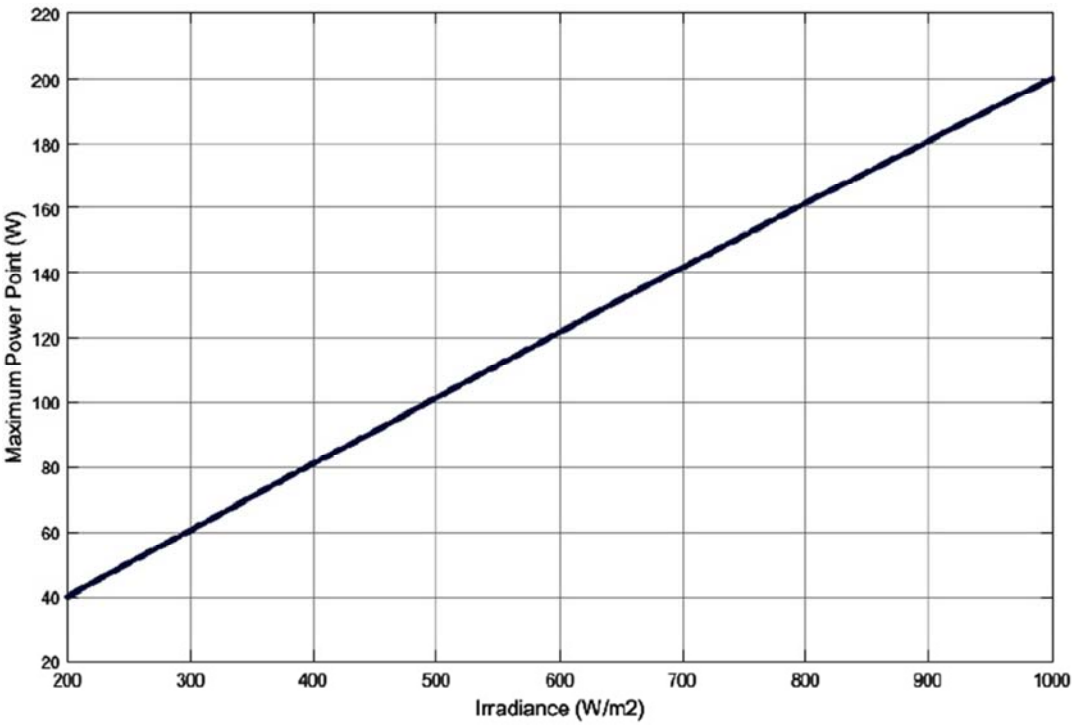

Figure 6. *Relationship of KC200GT Panel MPP with Radiation level.*

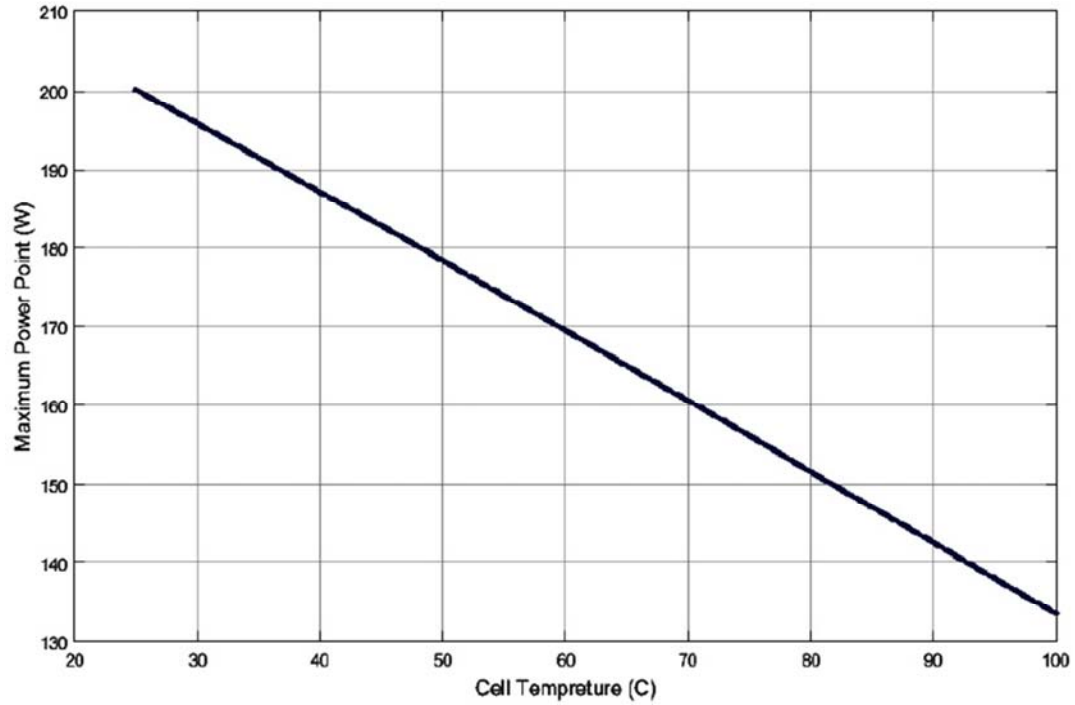

Figure 7. *Relationship of KC200GT Panel MPP with cell temperature.*

3.2. Coordinated Control Voltage-Frequency (v-f) and MPPT and Battery

The integrated voltage-frequency (v-f) and MPPT and battery control diagrams are shown in Figures 8 and 9, respectively [15]. The method consists of a control loop for MPPT control, two different loops for controlling v-f on the inverter side, and another loop for managing battery power. The loop 1 in Figure 8 is the MPPT control on the PV array side and uses the reference maximum power point (P_{MPPref}), Obtained from the MPP radiation table, with the actual PV output power (P_{PV}). And send the corresponding error to the controller PI (PI_1) whose output is the DC / DC converter incremental cycle (δ*). So by changing this cycle, the solar array will always be exploited at the reference point. The relation of this control loop is given in equation (8) where K_{p1} and K_{i1} are the proportional and integral gains of the

controller, respectively.

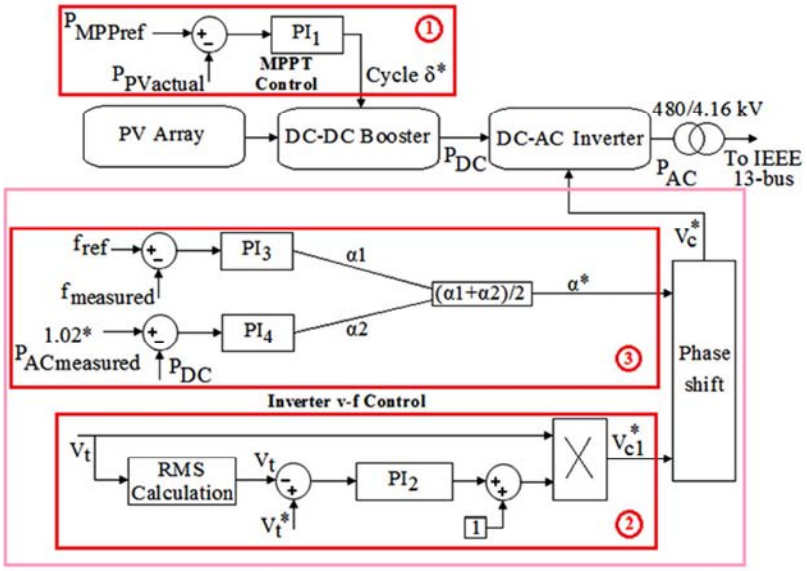

Figure 8. *Integrated v-f control diagram for PV with MPPT and battery [15].*

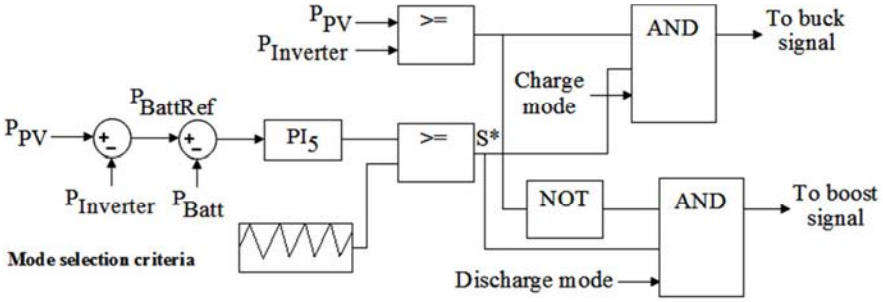

Figure 9. *Battery power control diagram [15].*

$$\delta^* = Kp1(Pmppref - Ppv) + Ki1\int_0^t (Pmppref - Ppv)dt \quad (8)$$

In order to control the voltage on the AC side, another feedback controller, PI_2, was used. As shown in Figure 8, in PCC loop 2 the voltage is measured and the effective value (rms) $V_t(t)$ is calculated, then this effective value is given by the reference voltage $V_t^*(t)$ which can be determined by the network., Is compared and the corresponding error is given to the PI controller. The output voltage of the inverter $V_c^*(t)$ is controlled so that it is in phase with the PCC voltage and its size is controlled to adjust the PCC voltage to the given level $V_t^*(t)$. This control scheme can be expressed specifically in relation (9):

$$V_c^* = v_t(t)\left[1 + K_{p2}(V_t^*(t) - V_t(t)) + K_{i2}\int_0^t (V_t^*(t) - V_t(t))\,dt\right] \quad (9)$$

Where, K_{p2} and K_{i2} are the proportional and integral gains of the controller, respectively. In Equation (9), the reason for adding 1 to the right of the equation is that when no power is injected into the PV system, the PV output voltage is exactly the same as the terminal voltage. Frequency control as shown in loop 3 is done by controlling the output power of the inverter side. The Microgrid reference frequency of 60 Hz is compared with the measured value and its error is given to the controller PI_3, which controls the α_1^* phase shift to displace the voltage waveform time scale to inject sufficient active power to maintain the frequency in the nominal value. It produces 60 Hz. The equation of this controller is as follows:

$$\alpha_1^* = K_{p3}(f_{ref} - f_{measured}) + K_{i3}\int_0^t (f_{ref} - f_{measured})\,dt \quad (10)$$

In loop 3 there is another controller, PI_4. This controller balances the active power between the AC and DC side of the inverter. Its reference signal is obtained from the dynamic changes of the active power injection from the AC side of the inverter is determined by the output of PI_3. The measured AC side power, $P_{ACmeasured}$, is multiplied by a factor of 1.02 to assume the inverter efficiency of 98% so that the DC side power is 102% of the AC side power. The two powers are compared with each other and the corresponding error is given to PI_4 to obtain the α_2^* phase shift of the loop whose relationship is as follows:

$$\alpha_2^* = K_{p4}(1.02P_{AC} - P_{DC}) + K_{i4}\int_0^t (1.02P_{AC} - P_{DC})\,dt \quad (11)$$

According to Equation (12) to achieve the final phase change (α*) of the voltage waveform (V_{c1}*), respectively, the average phase change on the DC and AC side, α_1* and α_2*, is calculated, which is then the reference voltage signal V_c* produces for inverter PWM switching scheme.

$$\alpha^* = \frac{(\alpha_1^* + \alpha_2^*)}{2} \quad (12)$$

The purpose here is to consider the phase shift of the active power of both the DC and AC side, control of the DC side voltage and obtain the desired value. If α_1* and α_2* have values near to the controller gain, it can be assured that the DC and AC power are in balance. This is coupled to a voltage control loop that ensures that the DC side voltage is maintained by the AC side voltage at optimum value.

The controllers, as well as those described above, are integrated with the battery power control in Figure 9. To supply or absorb the active power and frequency control by the PV system, a battery is used in the PV system configuration. If the solar power is high and the power required to control the frequency is less than the P_{MPP}, the battery will charge. If the available solar power is insufficient and the active power required to control the frequency is greater than the P_{MPP}, the battery will supply the power required to maintain the microprocessor frequency of 60 Hz.

The battery charge/discharge control method as outlined above and also considering the battery charge state (SOC) constraints are shown in Figure 9. This form, the Battery Reference Power ($P_{Battref}$) is dynamically generated by the difference between the injector inverter active power ($P_{inverter}$) and the PV Generation Power (P_{PV}). The controller consists of a PI_5 controller that receives the error signal after the difference between the battery active power and the reference power. To generate the S* signal, the signal obtained from PI_5 is compared to a triangular waveform of uniform size, which is similar to Pulse Width Modulation (PWM) in inverter control. K_{p5} and K_{i5} are the proportional and integral gains of the controller, respectively, and the equation of this control scheme is obtained from:

$$S^* = K_{p5}\left(P_{battref} - P_{batt}\right) + K_{i5}\int_0^t \left(P_{battref} - P_{batt}\right) dt \quad (13)$$

The next step is to distinguish between the battery charge and discharge mode, which results from comparing the P_{PV} to the $P_{inverter}$. If it is a $P_{PV} \geq P_{inverter}$, the battery is in a charged state and therefore, to generate the switching signal in order to enable the DC-DC converter buck mode, the signal from the PWM and S* must pass a logical AND.

If it is $P_{PV}<P_{inverter}$, it just the opposite signal and S* passes a logic AND in order to enable DC-DC converter boost mode and switching signal generation. With this control logic, the converter is capable of operating in both directions and can effectively charge or discharge the battery whenever needed.

4. Microgrid Configuration and Simulation Results

Figure 10 shows the diagram of the feeder distribution of the 13 IEEE bus studied along with the location of the PV array. This distribution feeder consists of one substation, 13 bus, 11 lines and eight loads. The loads consist of constant impedance, constant current and constant power (ZIP) types, most of which are constant power. In the Microgrid connected mode, the station is regarded as the source at the 650 bus and 115 kV level. In island mode, a diesel generator is set in the same bus as the reference set by the central controller (CC) of the Microgrid, to provide the active power at constant value.

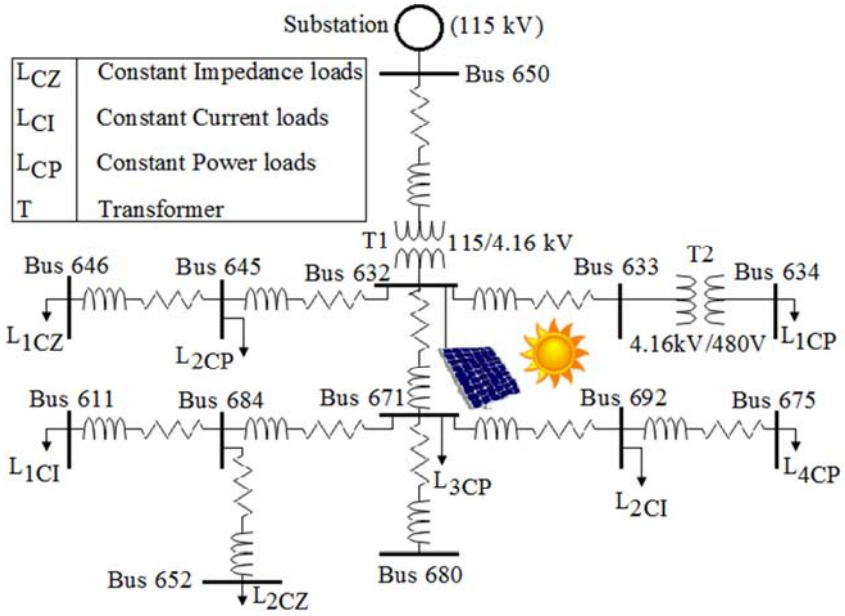

Figure 10. *The studied network [15].*

4.1. Testing of the Control Algorithm (v-f) in Islanded Microgrid

To evaluate the performance of the v-f control algorithm, two different radiation levels with radiation levels of 1000 and 750 W/ m^2 are considered as Scenario 1 and Scenario 2, respectively. The gains of PI controllers are presented in Table 2. During switching from network connection to island mode, a controlled diesel generator will be required to produce a certain amount of constant power according to the central controller command. In Figures 11 to 16 the integrated v-f control results in Scenario 1, Figures 17 to 22 the integrated v-f control results in Scenario 2 and Figures 23 to 26 the integrated v-f control results partnership with diesel generator.

According to Figure 11 and Figure 17, during the simulation period, the diesel generator produces a constant value of 1.25 MW. These figures also show the reactive power output of the diesel generator in kVar. In the island mode, too, the diesel generator's active power output is not sufficient to meet the demand for Microgrid power.

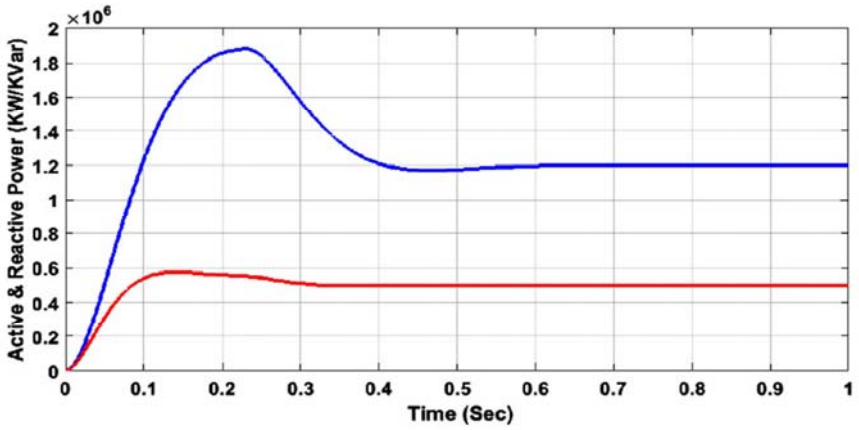

Figure 11. *Active and reactive power produced by diesel generator in scenario 1 (red curve: kVar, blue curve: kW).*

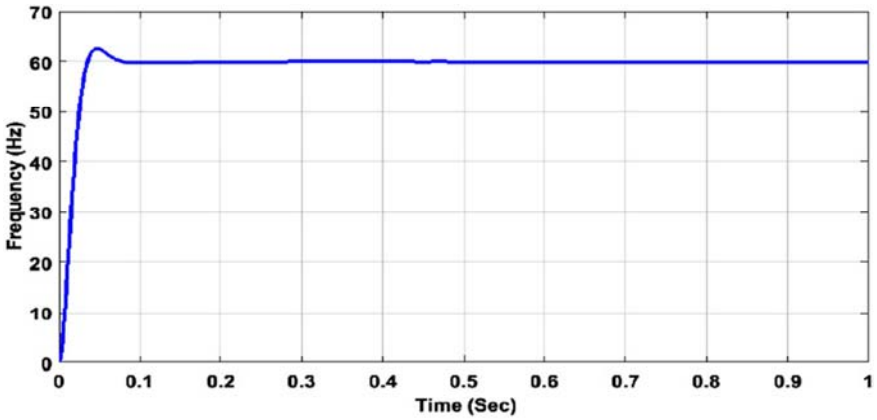

Figure 12. *Microgrid frequency in Scenario 1.*

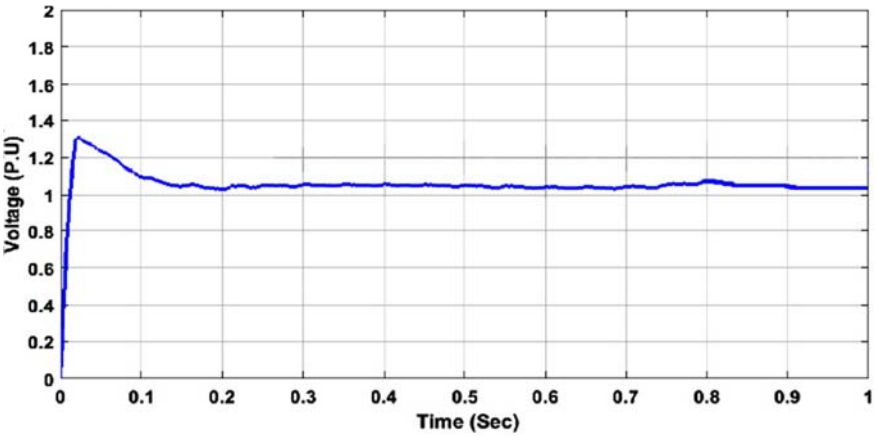

Figure 13. *PCC point voltage in scenario 1.*

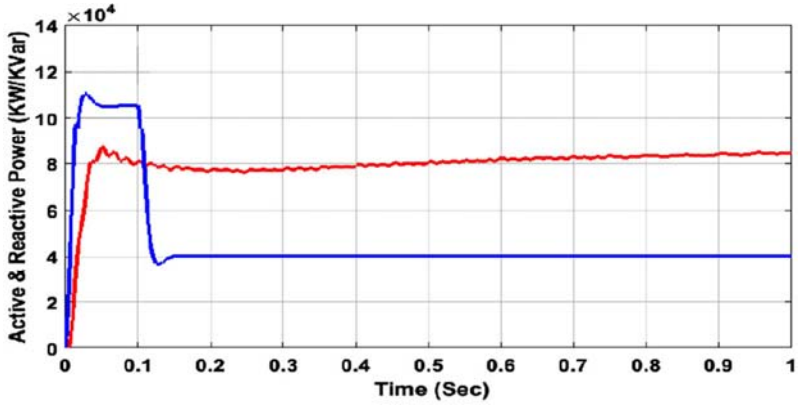

Figure 14. *Active and Reactive Injection PV Inverter in Scenario 1 (Red Curve: kW, Blue Curve: kVar).*

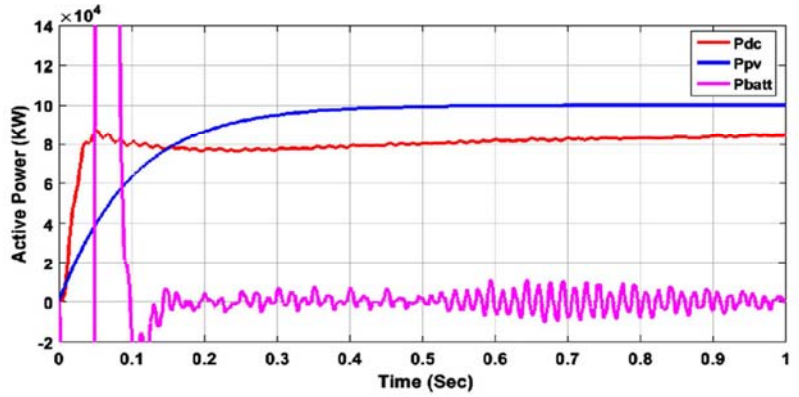

Figure 15. *The difference between the PV power and the battery in Scenario 1.*

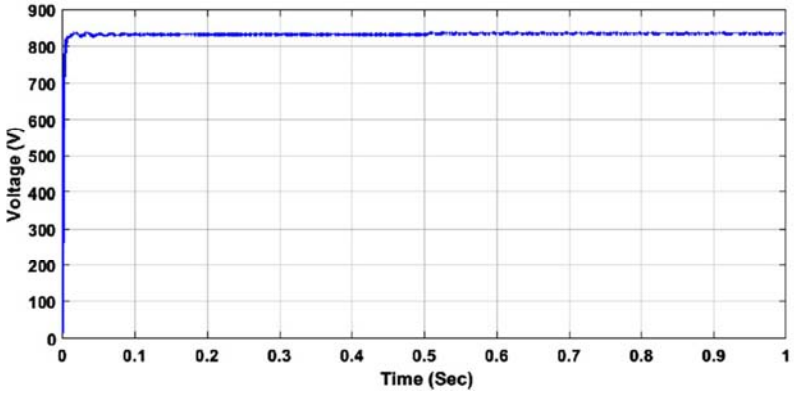

Figure 16. *DC voltage in scenario 1.*

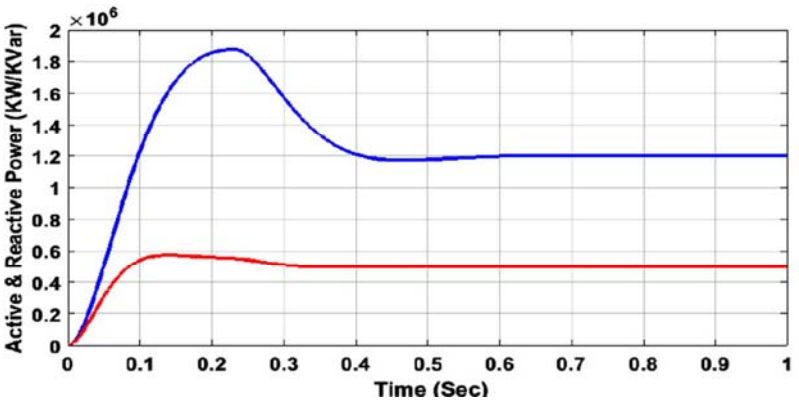

Figure 17. *Active and reactive power produced by diesel generator in scenario 2 (red curve: kVar, blue curve: kW).*

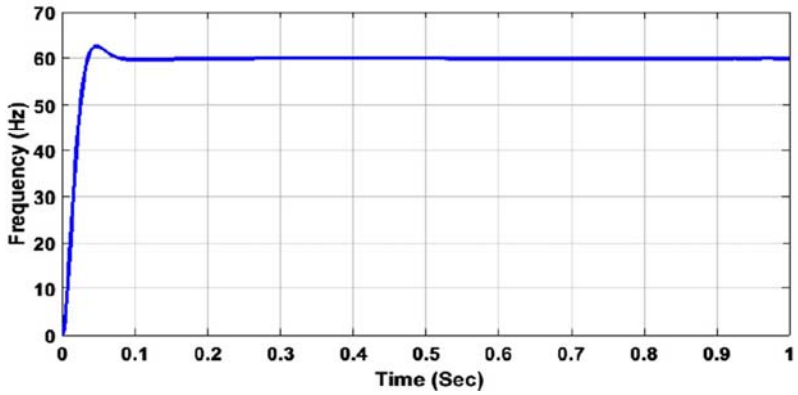

Figure 18. *Microgrid frequency in Scenario 2.*

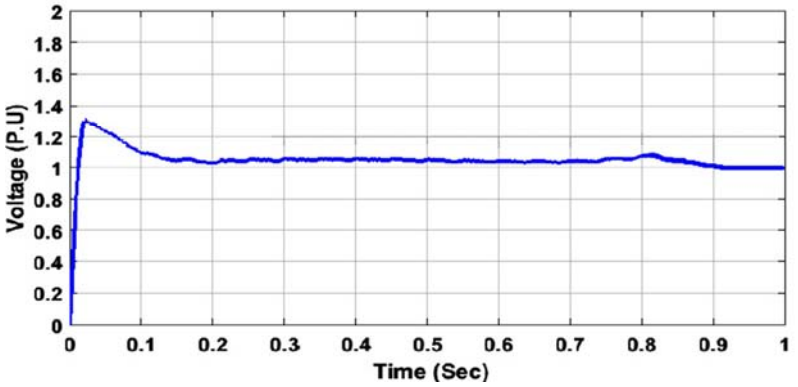

Figure 19. *PCC point voltage in scenario 2.*

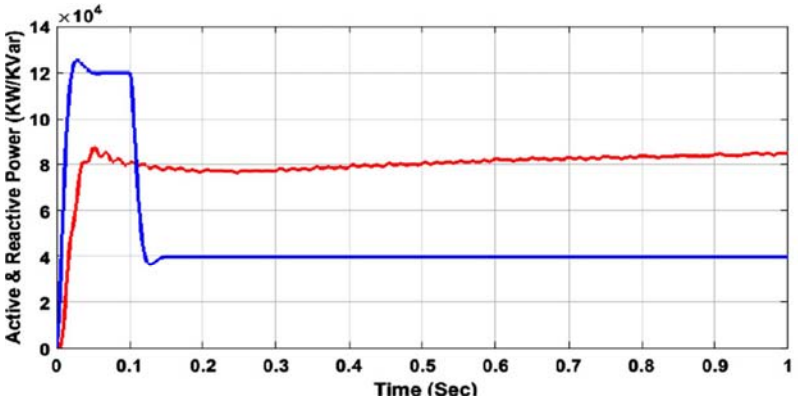

Figure 20. *Active and Reactive Injection PV Inverter in Scenario 2 (Red Curve: kW, Blue Curve: kVar).*

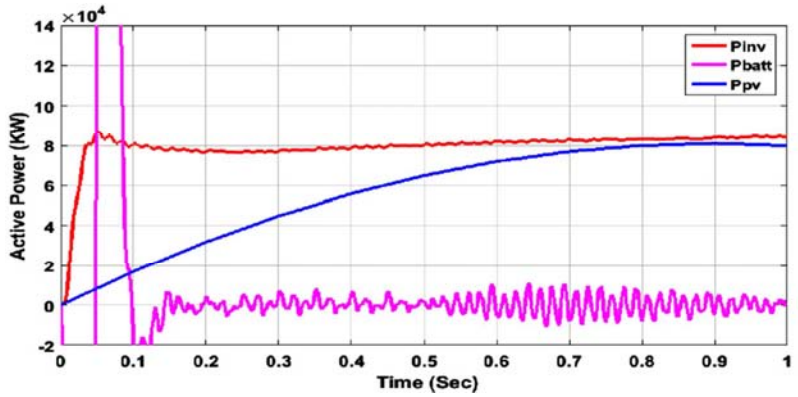

Figure 21. *The difference between the PV power and the battery in Scenario 2.*

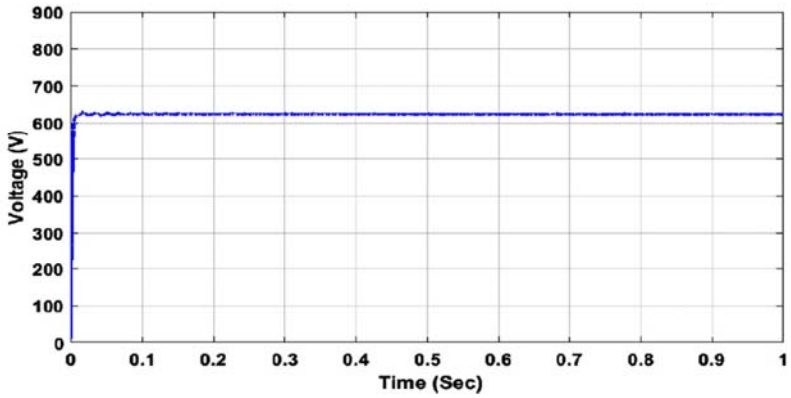

Figure 22. *DC voltage in scenario 2.*

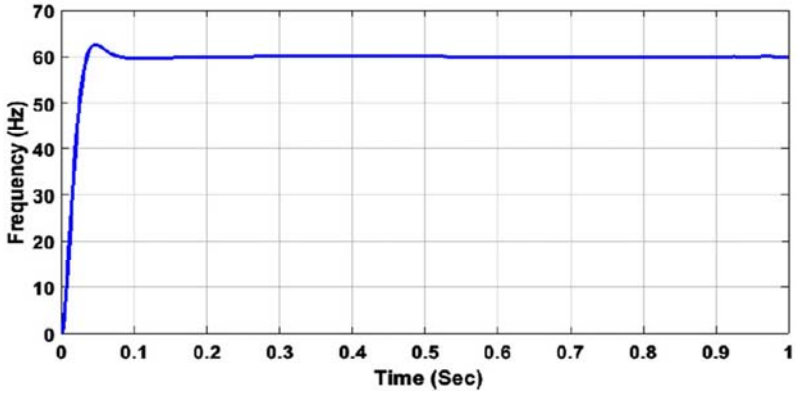

Figure 23. *Microgrid frequency in the presence of a diesel generator.*

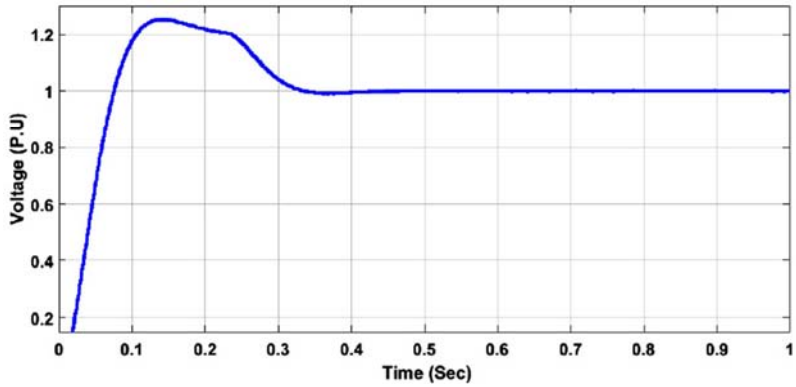

Figure 24. *Microgrid voltage in the presence of a diesel generator.*

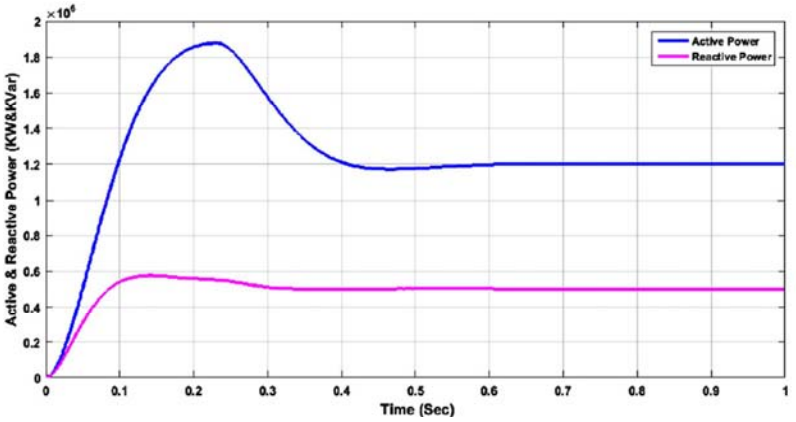

Figure 25. *Active and reactive power produced by diesel generator.*

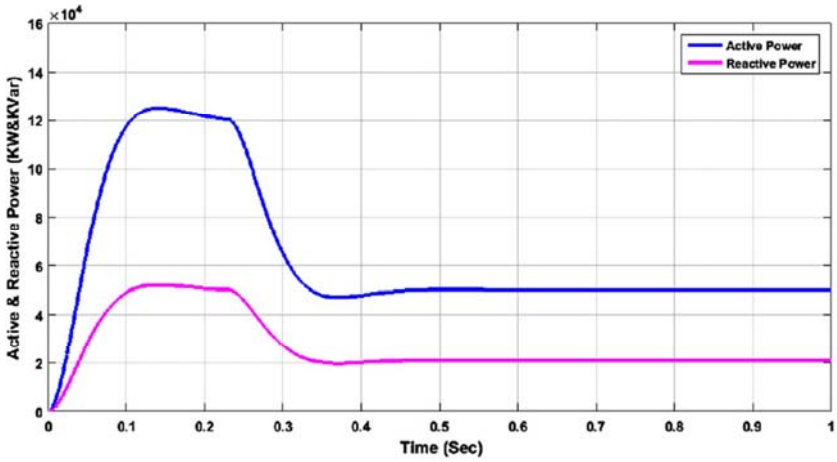

Figure 26. *Active and Reactive Injection PV Inverter in the presence of a diesel generator.*

Figure 12 and Figure 18 show the Microgrid frequency, which initially decreased to 57.8 Hz due to the imbalance between load and production. Frequency control of the PV system starts at 0.1 second, which quickly adjusts the frequency and returns it to 60 Hz in 0.2 seconds. Figure 13 and Figure 19 show the PCC voltage as per unit (pu). It can be seen that with the start of the control, the voltage is rapidly set to 1 per unit.

Figure 14 and Figure 20 show the active and reactive power of the PV inverter to regulate the voltage and frequency of the Microgrid. Injection of inverter active power to adjust the frequency of 60 Hz in both scenarios is about 80 kW. When providing this amount of power required for the Microgrid, there was a difference in the PV power share and battery energy storage as shown in Figure 15 and Figure 21.

Table 2. *Controller gains for v-f control [15].*

MPPT controller	K_{p1}	6×10^{-8}
	Ki1	6×10^{-6}
Voltage control	K_{p2}	0.0004
	Ki2	0.005
Frequency control	K_{p3}	9.9×10^{-4}
	Ki3	5×10^{-3}
PDC control	K_{p4}	0.8×10^{-9}
	Ki4	0.8×10^{-8}
Battery control	K_{p5}	1.5×10^{-8}
	Ki5	1.5×10^{-5}

In Scenario 1, the sun radiation is abundant and has the amount of 1000 W/m^2 and therefore the PV generates a maximum power of 100 kW which is higher than the value needed to maintain the frequency. That uses an extra 20 kW to charge the battery. A negative sign in battery power means charging and absorbing power.

In Scenario 2, due to reduced radiation levels, PV generates only about 75 kW in MPP, which is insufficient to maintain the Microgrid frequency of 60 Hz. Therefore, the power supply of about 5 kW is supplied by the battery as shown in Figure 21. A positive sign in battery power means the injection of active power into the grid.

Figure 16 and Figure 22 illustrates the DC voltage for the two scenarios mentioned above. It can be seen that the voltage for the two scenarios is maintained at about 850 V and 650 V, respectively.

Active power is generally balanced by the existence of controllers. This power balance coupled with AC side voltage control keeps the DC side voltage at a constant value which is the unique feature of the coordinated inverter control and the proposed MPPT.

4.2. Contribution of Diesel Generator to v-f Control

Figures 23 to 26 show is the results when a diesel generator is present in regulating the voltage and frequency of the Microgrid and controlling the PV system for generating constant and reactive power. The diesel generator v-f control also started in 0.2 seconds. Figure 23 shows the frequency of the Microgrid which initially increases abruptly and then gradually decreases and is fixed at 0.4 seconds at 60 Hz. Clearly, diesel generators take longer to recover than the combination of PV and Battery.

Figure 24 is the Microgrid voltage stabilized in about 0.5 seconds at 1 per unit. Figure 25 shows the diesel generator output power and Figure 26 shows the active and reactive power of the PV inverter operated in constant PQ mode.

It takes about 0.5 seconds for all the powers injected to stabilize and reach the desired level. It should be noted that the injection of PV inverter power is also affected by the diesel generator output power fluctuations in the initial seconds before reaching a steady-state.

Therefore, it is well proven that the battery and PV system without inertia of diesel generator, despite the inertia, is capable of fast and effective control of the voltage and frequency of the Microgrid.

5. Discussion

Today, fossil fuel restrictions and air pollution have created an incentive to use distributed generation resources and expand the technology. Power generation near the place of consumption, in addition to reducing system losses, can provide more flexibility to provide diverse services to

consumers [21-22]. One of the views proposed to effectively increase the contribution of these resources is the integration of these resources with the objectives of visibility, the proper connection between these resources and the electricity network, as well as the more efficient control of these resources. One of the ways to integrate distributed generation resources is a new concept called Microgrid. In the event of a disturbance in the network, the Microgrid is separated from the distribution network to isolate it from the disturbance in the network. This ability to create separate islands that have both production and consumption increases reliability over conventional networks and, on the other hand, provides better service, improved capacity and high security to subscribers.

Microgrid brings many benefits to consumers, including improved reliability by providing reliable power, by the island itself during power outages and improving power quality. In addition, the Microgrids reduce losses by shortening the production and consumption gap and managing blackouts, making the maintenance process very easy, as well as using renewable energy sources and renewable and clean energy and energy storage technologies, are many benefits to society.

The Microgrid control system is designed to safely and efficiently control and support the system's activities in two modes: island work and work as part of the electricity distribution network. This control system can be based on a central control system or can be scattered on any island forming a Microgrid. When the island is disconnected from the main network, the control system must control the local voltage level and frequency of production, calculate the difference between the generation and consumption of active and reactive power on the island, and take the necessary measures to stabilize the grid and the microgrid. Opposite maintain faults, incidents, shutdowns, and accidents and keep subscribers in optimum condition.

But for some reason, the power distribution companies are not going to the Microgrid right now. Some of the reasons are as follows:

1. Issues and problems related to quality control such as the existence of unusual voltage levels or the frequency outside the tolerable range of equipment [19].
2. Prevent the reconnection of the Microgrid to the main grid when there is a different voltage phase between the distribution network and the distributed generation resources in the Microgrid [16, 24].
3. Interference occurs when the island is connected to the distribution network [17].
4. Preventing accidents and hazards to the agents of power distribution companies when operating on lines that must not be electric, that but have become electrified due to the existence of Microgrid [18].
5. Due to safety and security issues in troubleshooting that may not be detected by the Microgrid systems [20].
6. Prevent condemnation of electricity distribution companies in matters and circumstances beyond their control [23].

But increasingly, economic incentives, technology growth, and environmental issues are changing the configuration and current layout of the electricity network from production to distribution. This paper presents a coordinated control technique for maintaining the voltage and frequency of the network in the islanded mode.

6. Conclusion

In this paper, a voltage-frequency control solution for a PV system with battery storage in an island Microgrid is presented. In this method, the PV system is operated at maximum power point and the battery storage is used to inject or absorb power through a charge/discharge cycle. The results show effective coordination between the v-f inverter control, MPPT control and battery storage control.

The results of the PV system control transition from v-f to constant power mode and the transfer of diesel generator control from constant power to frequency control have been satisfying. This feature helps the controller to adapt to changes in radiation levels as well as battery storage. The above-mentioned v-f control is much faster than a diesel generator to restore voltage and frequency to nominal value with diesel generator. In addition, calculations within the abc reference framework have made it easier and faster. Therefore, in general, installing a PV system with future battery storage can be very efficient in maintaining the voltage and frequency of the Microgrid.

References

[1] Adhikari, Sarina, Fangxing Li, and Huijuan Li. "PQ and PV control of photovoltaic generators in distribution systems." *IEEE Transactions on Smart Grid* 6, no. 6 (2015): 2929-2941.

[2] Lasseter, Robert H. "Microgrids." In *2002 IEEE Power Engineering Society Winter Meeting. Conference Proceedings (Cat. No. 02CH37309)*, vol. 1, pp. 305-308. IEEE, 2002.

[3] Zamora, Ramon, and Anurag K. Srivastava. "Controls for microgrids with storage: Review, challenges, and research needs." *Renewable and Sustainable Energy Reviews* 14, no. 7 (2010): 2009-2018.

[4] Lopes, JA Peças, C. L. Moreira, and A. G. Madureira. "Defining control strategies for microgrids islanded operation." *IEEE Transactions on power systems* 21, no. 2 (2006): 916-924.

[5] Marwali, Mohammad N., Jin-Woo Jung, and Ali Keyhani. "Control of distributed generation systems-Part II: Load sharing control." *IEEE Transactions on power electronics* 19, no. 6 (2004): 1551-1561.

[6] Vásquez, Juan C., Josep M. Guerrero, Eduard Gregorio, Pedro Rodríguez, Remus Teodorescu, and Frede Blaabjerg. "Adaptive droop control applied to distributed generation inverters connected to the grid." In *2008 IEEE International Symposium on Industrial Electronics*, pp. 2420-2425. IEEE, 2008.

[7] Bevrani, Hassan, and Shoresh Shokoohi. "An intelligent droop control for simultaneous voltage and frequency regulation in islanded microgrids." *IEEE transactions on smart grid* 4, no. 3 (2013): 1505-1513.

[8] Vasquez, Juan C., Josep M. Guerrero, Mehdi Savaghebi, Joaquin Eloy-Garcia, and Remus Teodorescu. "Modeling, analysis, and design of stationary-reference-frame droop-controlled parallel three-phase voltage source inverters." *IEEE Transactions on Industrial Electronics* 60, no. 4 (2012): 1271-1280.

[9] Vandoorn, Tine L., Bart Meersman, Jeroen DM De Kooning, and Lieven Vandevelde. "Analogy between conventional grid control and islanded microgrid control based on a global DC-link voltage droop." *IEEE transactions on power delivery* 27, no. 3 (2012): 1405-1414.

[10] Vasquez, Juan C., Rosa A. Mastromauro, Josep M. Guerrero, and Marco Liserre. "Voltage support provided by a droop-controlled multifunctional inverter." IEEE Transactions on Industrial Electronics 56, no. 11 (2009): 4510-4519.

[11] Watson, Luke D., and Jonathan W. Kimball. "Frequency regulation of a microgrid using solar power." In *2011 Twenty-Sixth Annual IEEE Applied Power Electronics Conference and Exposition (APEC)*, pp. 321-326. IEEE, 2011.

[12] Villalva, Marcelo Gradella, Jonas Rafael Gazoli, and Ernesto Ruppert Filho. "Comprehensive approach to modeling and simulation of photovoltaic arrays." *IEEE Transactions on power electronics* 24, no. 5 (2009): 1198-1208.

[13] Xu, Yan, Huijuan Li, D. Tom Rizy, Fangxing Li, and John D. Kueck. "Instantaneous active and nonactive power control of distributed energy resources with a current limiter." In *2010 IEEE Energy Conversion Congress and Exposition*, pp. 3855-3861. IEEE, 2010.

[14] Tremblay, Olivier, and Louis-A. Dessaint. "Experimental validation of a battery dynamic model for EV applications." *World electric vehicle journal* 3, no. 2 (2009): 289-298.

[15] Adhikari, Sarina, and Fangxing Li. "Coordinated Vf and PQ control of solar photovoltaic generators with MPPT and battery storage in microgrids." *IEEE Transactions on Smart grid* 5, no. 3 (2014): 1270-1281.

[16] Dashtdar, Majid, and Masoud Dashtdar. "Voltage control in distribution networks in presence of distributed generators based on local and coordinated control structure." *The Scientific Bulletin of the Electrical Engineering Faculty - SBEEF* 3, no. 1 (2019): 30-37.

[17] Rajesh, K. S., S. S. Dash, R. Sridhar, and Ragam Rajagopal. "Implementation of an adaptive control strategy for solar photovoltaic generators in microgrids with MPPT and energy storage." In 2016 IEEE International Conference on Renewable Energy Research and Applications (ICRERA), pp. 766-771. IEEE, 2016.

[18] Rajanna, B. V., S. V. N. L. Lalitha, Ganta Joga Rao, and S. K. Shrivastava. "Solar Photovoltaic Generators with MPPT and Battery Storage in Microgrids." *International Journal of Power Electronics and Drive Systems* 7, no. 3 (2016): 701.

[19] Xu, Ling, Zhixin Miao, and Lingling Fan. "Coordinated control of a solar and battery system in a microgrid." In *PES T&D 2012*, pp. 1-7. IEEE, 2012.

[20] Hosseinimoghadam, Seyed Mohammad Sadegh, Masoud Dashtdar, Majid Dashtdar, and Hamzeh Roghanian. "SECURITY CONTROL OF ISLANDED MICRO-GRID BASED ON ADAPTIVE NEURO-FUZZY INFERENCE SYSTEM." *"Scientific Bulletin": Series C Electrical Engineering and Computer Science*, no. 1 (2020): 189-204.

[21] Najafi, M., Ahmadi, S. and Dashtdar, M., Simultaneous Energy and Reserve Market Clearing with Consideration of Interruptible Loads as One of Demand Response Resources and Different Reliability Requirements of Consumers. *International Journal of Emerging Electric Power Systems*, *20* (5).

[22] Dashtdar, M., Najafi, M. and Esmaeilbeig, M., 2020. Calculating the locational marginal price and solving optimal power flow problem based on congestion management using GA-GSF algorithm. *Electrical Engineering*, pp. 1-18.

[23] Dashtdar, Majid, and Masoud Dashtdar. "Power control in an islanded microgrid using virtual impedance." *The Scientific Bulletin of Electrical Engineering Faculty* 19, no. 1 (2020): 21-27.

[24] Dashtdar, Masoud, Mojtaba Najafi, and Mostafa Esmaeilbeig. "Probabilistic planning for participation of virtual power plants in the presence of the thermal power plants in energy and reserve markets." *Sadhana* 45, no. 1 (2020).